ACS APPLIED MATERIALS & INTERFACES

Research Article

www.acsami.org

High Crystalline Dithienosilole-Cored Small Molecule Semiconductor for Ambipolar Transistor and Nonvolatile Memory

Woonggi Kang,[†,#] Minwoo Jung,[‡,§,#] Wonsuk Cha,[∥] Sukjae Jang,[†] Youngwoon Yoon,[‡] Hyunjung Kim,[∥] Hae Jung Son,[‡] Doh-Kwon Lee,[‡] BongSoo Kim,*[,‡] and Jeong Ho Cho*[,†]

[†]SKKU Advanced Institute of Nanotechnology (SAINT), School of Chemical Engineering, Sungkyunkwan University, Suwon 440-746, Republic of Korea

[‡]Photo-electronic Hybrids Research Center, Korea Institute of Science and Technology (KIST), Seoul 136-791, Republic of Korea

[§]Department of Chemistry, Korea University, Seoul 136-713, Republic of Korea

[∥]Department of Physics, Sogang University, Seoul 121-742, Republic of Korea

Supporting Information

ABSTRACT: We characterized the electrical properties of a field-effect transistor (FET) and a nonvolatile memory device based on a solution-processable low bandgap small molecule, Si1TDPP-EE-C6. The small molecule consisted of electron-rich thiophene-dithienosilole-thiophene (Si1T) units and electron-deficient diketopyrrolopyrrole (DPP) units. The as-spun Si1TDPP-EE-C6 FET device exhibited ambipolar transport properties with a hole mobility of 7.3×10^{-5} $cm^2/(V\ s)$ and an electron mobility of 1.6×10^{-5} $cm^2/(V\ s)$. Thermal annealing at 110 °C led to a significant increase in carrier mobility, with hole and electron mobilities of 3.7×10^{-3} and 5.1×10^{-4} $cm^2/(Vs)$, respectively. This improvement is strongly correlated with the increased film crystallinity and reduced $\pi-\pi$ intermolecular stacking distance upon thermal annealing, revealed by grazing incidence X-ray diffraction (GIXD) and atomic force microscopy (AFM) measurements. In addition, nonvolatile memory devices based on Si1TDPP-EE-C6 were successfully fabricated by incorporating Au nanoparticles (AuNPs) as charge trapping sites at the interface between the silicon oxide (SiO_2) and cross-linked poly(4-vinylphenol) (*c*PVP) dielectrics. The device exhibited reliable nonvolatile memory characteristics, including a wide memory window of 98 V, a high on/off-current ratio of 1×10^3, and good electrical reliability. Overall, we demonstrate that donor−acceptor-type small molecules are a potentially important class of materials for ambipolar FETs and nonvolatile memory applications.

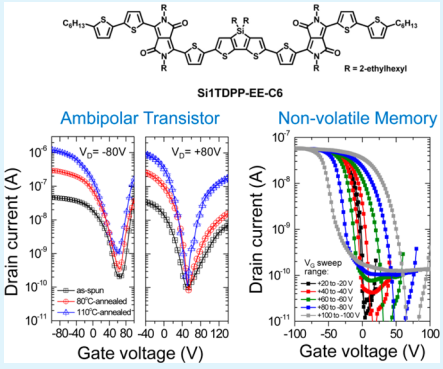

KEYWORDS: *donor−acceptor-type small molecules, ambipolar field effect transistor, nonvolatile memory, crystallinity, hole mobility, charge trapping*

1. INTRODUCTION

Organic field-effect transistors (OFETs) have great potentials for their use in large-area flexible displays, radiofrequency identification (RF-ID) tags, and memory devices because of their solution processability and high compatibility with flexible substrates and thus have been intensively investigated.[1−5] Realizing large-area flexible OFETs requires high-performance and solution-processable organic electronic components, such as conducting, semiconducting, and dielectric materials.[6−11] Among these components, the development of new semiconducting channel materials is of paramount importance.

A number of donor−acceptor-type low-bandgap polymers composing of electron-rich donor and electron-deficient acceptor blocks have been developed for semiconducting channel materials in OFETs. For instance, thiophenes[12] and selenophenes[13] are good electron-rich donors and isoindigos,[14,15] diketopyrrolopyrroles (DPP),[16,17] benzothiadiazoles,[4,18] and naphthalenedicarboximide[19] are well-known electron-deficient acceptor blocks. Especially, DPP-based polymers have emerged as a promising class of donor−acceptor-type polymers, which exhibited high carrier mobilities over 1 $cm^2/(Vs)$ due to the strong $\pi-\pi$ interactions among planar electron-deficient DPP moieties.[20,21] OFETs constituted with DPP-based polymers often showed ambipolar behavior presumably because their HOMO and LUMO levels lie close to the Fermi levels of source/drain electrodes.[22,23] It should be noted that ambipolar semiconductor allows the simple fabrication of complementary metal oxide semiconductor (CMOS)-like inverters without complex micropatterning of n-channel and p-channel semiconducting materials.[24−31]

Recently, solution-processable small molecules have become an emerging and promising set of alternatives to donor−acceptor-type polymers. These compounds offer a straightforward synthesis, are easily purified and functionalized, do not

Received: January 11, 2014
Accepted: April 7, 2014
Published: April 7, 2014

Scheme 1. Synthesis of the Si1TDPP-EE-C6

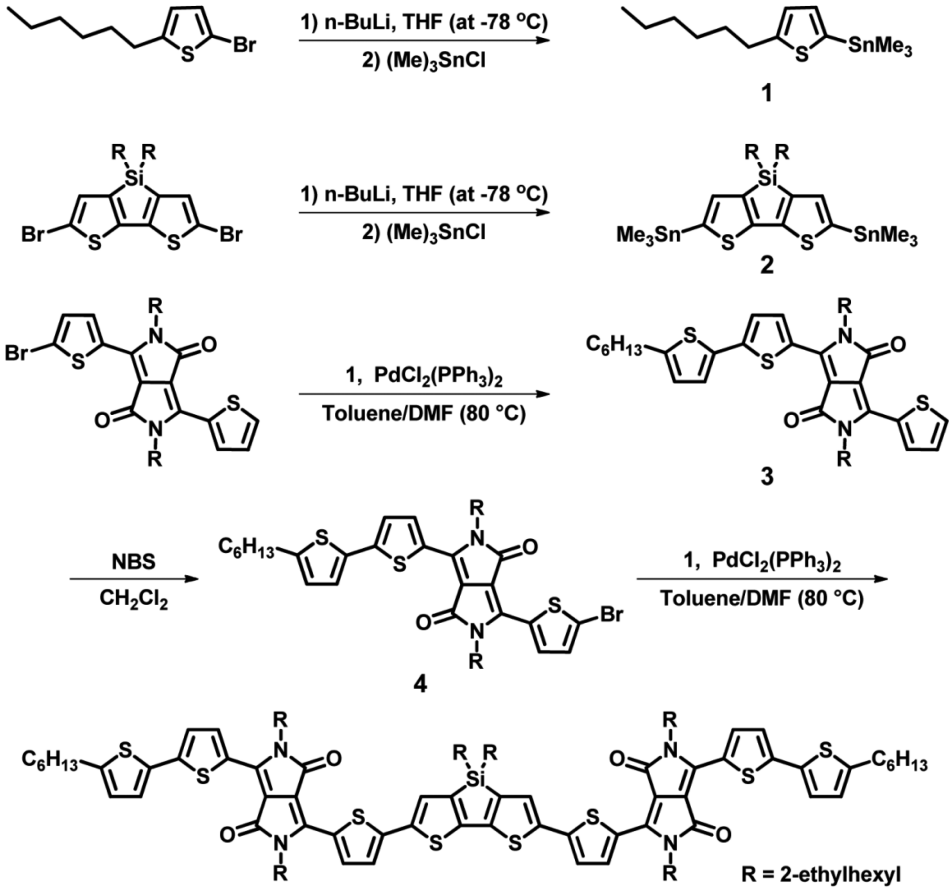

suffer from batch-to-batch variation, and are intrinsically monodisperse.[32−37] Despite these advantages, only one report has described the successful demonstration of ambipolar behavior from donor−acceptor-type small molecules, to the best of our knowledge.[37] Moreover, although solution-processable conjugated small molecules are potentially useful in transistor-type nonvolatile memory devices that function by trapping charges in the dielectric layers, they have not been explored for such applications.

In this paper, we report the synthesis, characterization, and device properties of a low bandgap silole-based small molecular semiconductor, Si1TDPP-EE-C6, containing electron-rich thiophene−dithienosilole−thiophene (Si1T) units and electron-deficient diketopyrrolopyrrole (DPP) units. The combination of Si1T and DPP units was chosen because (i) 2-ethylhexyl chained dithienosilole groups as well as thiophenes were known to be good electron-donating units and also promote very close $\pi-\pi$ stacking[38,39] and DPP moieties would act as an excellent electron-deficient units as explained above. Synthetic routes to this molecule are shown in Scheme 1. The as-spun Si1TDPP-EE-C6 exhibited ambipolar transport characteristics and thermal annealing increased carrier mobilities significantly because it increased the film crystallinity and facilitated the close intermolecular stacking. Moreover, the Si1TDPP-EE-C6 molecule was successfully used as an active channel material for nonvolatile memory devices where Au nanoparticles (AuNPs) were embedded between SiO_2 layers and cross-linked poly(4-vinylphenol) (*c*PVP) dielectric layers. The resulting device exhibited reliable nonvolatile memory characteristics and good electrical reliability.

2. EXPERIMENTAL SECTION

2.1. Materials and synthesis. 2-Bromo-5-hexylthiophene, *N*-bromosuccinimde (NBS), 1.6 M *n*-butyllithium (BuLi) solution in hexanes, *N*,*N*,*N*′,*N*′-tetramethylethylenediamine (TMEDA), 1.0 M trimethyltinchloride solution in tetrahydrofuran (THF), and bis-(triphenylphosphine)palladium(II) dichoride ($PdCl_2(PPh_3)_2$) were purchased from Aldrich and TCI. 3-(5-Bromothiophen-2-yl)-2,5-bis(2-ethylhexyl)-6-(thiophen-2-yl)pyrrolo[3,4-*c*]pyrrole-1,4(2*H*,5*H*)-dione was purchased from Lumtec. Common organic solvents were purchased from Daejung and J. T. Baker. THF was dried over sodium and benzophenone prior to use. All other solvents (toluene, DMF, CH_3OH, and $CHCl_3$) were used as received without further purification.

*Synthesis of (5-hexylthiophen-2-yl)trimethylstannane (**1**).* 2-Bromo-5-hexylthiophene (1.0 g, 4.05 mmol) was added to a 50 mL frame-dried reaction tube with a magnetic bar. Ten milliliters of anhydrous THF as solvent was added to the reaction tube, which was then cooled to −78 °C using a dry ice/acetone bath. 1.6 M *n*-BuLi solutionin hexane (6.32 mL, 10.11 mmol) and TMEDA (1.52 mL, 10.11 mmol) were added slowly. The reaction mixture was warmed up to 0 °C slowly and stirred for 2 h. The reaction mixture was cooled again to −78 °C and 1.0 M trimethyltinchloride solution in THF (10.11 mL, 10.11 mmol) was added to the reaction mixture slowly. This mixture was warmed up to RT gradually and stirred for 8 h. After reaction completion, 50 mL of H_2O was added to the reaction mixture, which was extracted with 200 mL of $CHCl_3$ three times. The combined organic layer was dried over anhydrous $MgSO_4$. The solvent

was evaporated to yield yellowish oil compound **1**. (The product was used for next reaction without further purification) Yield: 1.2 g, 93%. ^{1}H NMR (CD_2Cl_2, δ ppm) 0.27−0.42 (m, 9H), 0.91 (m, 3H), 1.32−1.38 (m, 6H), 1.68 (m, 2H), 2.84−2.88 (m, 2H), 6.90 (s, 1H, aromatic proton), 7.05 (s, 1H, aromatic proton)

*Synthesis of 4,4-bis(2-ethylhexyl)-2,6-bis(trimethylstannyl)-4H-silolo[3,2-b:4,5-b′]dithiophene (**2**).* 2,6-Dibromo-4,4-bis(2-ethylhexyl)-4H-silolo[3,2-*b*:4,5-*b*′]dithiophene (1.0 g, 1.73 mmol) was added to a 50 mL frame-dried reaction tube with a magnetic bar. Fifteen milliliters of anhydrous THF was added to the reaction tube, which was then cooled to −78 °C using a dry ice/acetone bath. 1.6 M *n*-BuLi solution in hexane (2.71 mL, 4.34 mmol) and TMEDA (0.65 mL, 4.34 mmol) were added slowly. The reaction mixture was warmed up to 0 °C slowly and stirred for 2 h. The reaction mixture was cooled again to −78 °C and 1.0 M trimethyltin chloride solution in THF (4.34 mL, 4.34 mmol) was added to the reaction mixture slowly. This mixture was warmed up to RT gradually and stirred for 8 h. After reaction completion, 50 mL of H_2O was added to the reaction mixture, which was extracted with 200 mL of $CHCl_3$ three times. The combined organic layer was dried over anhydrous $MgSO_4$. The solvent was evaporated to yield brown oil compound **2**. (The product was used for the next reaction without further purification.) Yield: 1.2 g, 91%. ^{1}H NMR ($CDCl_3$, δ ppm) 0.29−0.44 (m, 18H), 0.75−0.90 (m, 12H), 0.90−0.99 (m, 2H), 1.15−1.30 (m, 16H), 1.40−1.53 (m, 4H), 7.07 (s, 2H, aromatic proton)

*Synthesis of 3-(5-bromothiophen-2-yl)-2,5-bis(2-ethylhexyl)-6-(thiophen-2-yl)pyrrolo[3,4-c]pyrrole-1,4(2H,5H)-dione (**3**).* To a 100 mL flame-dried reaction tube with a magnetic bar were added compound **1** (645 mg, 1.948 mmol), 3-(5-bromothiophen-2-yl)-2,5-bis(2-ethylhexyl)-6-(thiophen-2-yl)pyrrolo[3,4-*c*]pyrrole-1,4(2*H*,5*H*)-dione (980 mg, 1.62 mmol), 20 mL of anhydrous toluene, and 5 mL of anhydrous DMF. The reaction solution was degassed by three freeze−pump−thaw cycles. Bis(triphenylphosphine)palladium(II) dichoride ($PdCl_2(PPh_3)_2$) (57 mg, 0.081 mmol) was then added to the reaction mixture, which was stirred at 90 °C for 4 h. After reaction completion, the reaction mixture was cooled to RT and poured into 200 mL of methanol to yield red colored precipitates. The precipitates were filtered and purified by column chromatography using an eluent of DCM:hexane (1:1, v/v) to give a black solid compound **3**. Yield: 900 mg, 73%. ^{1}H−NMR ($CDCl_3$, δ ppm) 0.85−0.90 (m, 15H), 1.20−1.36 (m, 22H), 1.66−1.71 (m, 2H), 1.85−1.90 (m, 2H), 2.80−2.84 (m, 2H), 4.02−4.04 (m, 4H), 6.75 (d, 1H, J = 3.6 Hz, aromatic proton), 7.14 (d, 1H, J = 3.6 Hz, aromatic proton), 7.24 (d, 1H, J = 4.8 Hz, aromatic proton), 7.26 (d, 1H, J = 4.8 Hz, aromatic proton), 7.61(d, 1H, J = 5.2 Hz, aromatic proton), 8.86 (d, 1H, J = 4.0 Hz, aromatic proton), 8.95 (d, 1H, J = 4.4 Hz, aromatic proton).

*Synthesis of 3-(5-bromothiophen-2-yl)-2,5-bis(2-ethylhexyl)-6-(5′-hexyl-[2,2′-bithiophen]-5-yl)pyrrolo[3,4-c]pyrrole-1,4(2H,5H)-dione (**4**).* To a 100 mL round bottomed flask with a magnetic bar were added compound **3** (1.07 g, 1.548 mmol) and 20 mL of dichloromethane. The reaction mixture was cooled to 0 °C using an iced water bath. NBS (331 mg, 1.858 mmol) was added to flask in one portion and the reaction mixture was stirred at 0 °C for 2 h. After the reaction was finished, 200 mL of H_2O was added to the mixture, which was extracted with 200 mL of $CHCl_3$ three times. The combined organic layer was dried over anhydrous $MgSO_4$ and the solvent was evaporated under reduced pressure. The crude product was purified by column chromatography using an eluent of $CHCl_3$:hexane (1:1, v/v) to yield a dark reddish solid compound **4**. Yield: 1.1 g, 92%. ^{1}H−NMR (CD_2Cl_2, δ ppm) 0.88−0.91 (m, 15H), 1.28−1.37 (m, 22H), 1.67−1.72 (m, 2H), 1.83−1.91 (m, 2H), 2.82−2.86 (m, 2H), 3.93−4.03 (m, 4H), 6.79 (d, 1H, J = 3.2 Hz, aromatic proton), 7.19 (d, 1H, J = 3.6 Hz, aromatic proton), 7.26 (d,1H, J = 4.4 Hz, aromatic proton), 7.28 (d, 1H, J = 4.4 Hz, aromatic proton), 8.59 (d, 1H, J = 4.0 Hz, aromatic proton), 8.95 (d, 1H, J = 4.0 Hz, aromatic proton).

Synthesis of 6,6′-(5,5′-(4,4-bis(2-ethylhexyl)-4H-silolo[3,2-b:4,5-b′]dithiophene-2,6-diyl)bis(thiophene-5,2-diyl))bis(2,5-bis(2-ethylhexyl)-3-(5′-hexyl-[2,2′-bithiophen]-5-yl)pyrrolo[3,4-c]pyrrole-1,4-(2H,5H)-dione) (Si1TDPP-EE-C6). To a 25 mL flame-dried reaction tube with a magnetic bar were added compound 2 (106 mg, 0.143 mmol), compound **4** (231 mg, 0.300 mmol), 8 mL of anhydrous toluene, and 2 mL of anhydrous DMF. The reaction solution was degassed by three freeze−pump−thaw cycles. Bis-(triphenylphosphine)palladium(II) dichoride ($PdCl_2(PPh_3)_2$) (5 mg, 0.007 mmol) was then added to the reaction mixture, which was stirred at 90 °C for 8 h. After reaction completion, reaction mixture was cooled to RT and poured into 100 mL of methanol to yield black-colored precipitates. The precipitates were filtered and purified by column chromatography using an eluent of $CHCl_3$:hexane (1:1, v/v) to give a desired black solid. Yield: 150 mg, 58%. ^{1}H−NMR (CD_2Cl_2, δ ppm) 0.83−0.92 (m, 42H), 1.05 (m, 4H), 1.20−1.40 (m, 62H), 1.66−1.71 (m, 4H), 1.91 (m, 4H), 2.71−2.85 (m, 4H), 4.02 (m, 8H), 6.77 (d, 2H, J = 3.6 Hz, aromatic proton), 7.16 (d, 2H, J = 3.6 Hz, aromatic proton), 7.22 (d, 2H, J = 4.0 Hz, aromatic proton), 7.28 (d, 2H, J = 4.4 Hz, aromatic proton), 7.34 (s, 2H, aromatic proton), 8.90 (d, 2H, J = 4.0 Hz, aromatic proton), 8.94 (d, 2H, J = 4.4 Hz, aromatic proton). MS (MALDI-TOF), $[M + H]^+$, 1797.8; Found, 1798.2 (Figures S1 and S2 in the Supporting Information show ^{1}H−NMR and MALDI-TOF spectra, respectively).

2.2. Material Characterization. ^{1}H NMR spectra were taken using a Bruker Advance 400 spectrometer (400 MHz). Molecular weights were measured by matrix-assisted laser desorption/ionization time-of-flight mass spectrometry (MALDI-TOF MS), performed on a Bruker Autoflex instrument. Differential scanning calorimetry (DSC) measurements were conducted using a PerkinElmer Pyris 1 DSC instrument (heating rate = 10 °C/min, under nitrogen). UV−visible absorption spectra were taken on a PerkinElmer Lamb 9 UV−vis spectrophotometer. Cyclic voltammograms were recorded on a CH instrument electrochemical analyzer (scan rate =50 mV/s). A degassed acetonitrile containing 0.1 M tetrabutylammonium hexafluorophosphate ($TBAPF_6$) was used as an electrolyte solution. The working electrode was the Si1TDPP-EE-C6 coated Pt wire, the counter electrode a Pt wire, and the reference electrode Ag/Ag^+. The reference electrode potential was calibrated with the Fc/Fc^+ potential, which was assumed to be 4.8 eV below the vacuum level.[40] The crystalline characteristics of the Si1TDPP-EE-C6 films were investigated by GIXD measurements at the 8-ID-E beamline of the Advanced Photon Source (APS) at Argonne National Laboratory, USA. The surface morphologies of the Si1TDPP-EE-C6 films were examined by tapping mode AFM (D3100 Nanoscope V, Veeco). Electrical properties of the OFETs were recorded using Keithley 2400 and 236 source/measure units under vacuum (1×10^{-5} Torr) and in dark.

2.3. Device Fabrication. OFETs and nonvolatile memory devices based on Si1TDPP-EE-C6 were fabricated on a substrate comprising a highly doped n-type Si wafer (gate electrode) onto which a 300 nm thick silicon oxide (SiO_2) layer (gate insulator) was thermally grown. After cleaning the Si wafer in piranha solution (30 min, 100 °C) and washing with distilled water, the SiO_2 surface was modified with octadecyltrichlorosilane (ODTS, Gelest, Inc.) to reduce electron trapping by the silanol groups on the SiO_2. The water contact angle of the ODTS-treated surfaces was 112°. The nonvolatile memory device was fabricated by thermally depositing a 1 nm thick Au layer onto the SiO_2 layer. The substrate was subsequently annealed at 100 °C for 10 min to form the AuNPs. A layer of poly(4-vinylphenol) (PVP) mixed with a poly(melamine-*co*-formaldehyde) (PMF) cross-linking agent (in a weight ratio of 2:1) was spin-coated onto the SiO_2 layer bearing AuNPs at 150 °C for 1 h for cross-linking of PVP. To form the semiconductor layer for OFET and nonvolatile memory, a 40 nm thick Si1TDPP-EE-C6 film was spin-cast using a 0.5 wt % chloroform solution onto the ODTS-treated SiO_2 substrate or the cross-linked PVP (*c*PVP)/AuNPs/SiO_2, respectively. The spin-cast films were dried in a vacuum chamber (24 h) and then thermally annealed for 30 min in a vacuum chamber at 25, 80, and 110 °C. Finally, Au source/drain electrodes with a thickness of 50 nm were thermally vacuum-deposited through a shadow mask onto the Si1TDPP-EE-C6 film. The channel length and width were 50 and 800 μm, respectively.

3. RESULTS AND DISCUSSION

Scheme 1 shows the synthetic route of the low-bandgap small molecule, Si1TDPP-EE-C6. The optical electronic properties of Si1TDPP-EE-C6 were measured using cyclic voltammetry and UV−visible absorption spectroscopy. The cyclic voltammogram of Si1TDPP-EE-C6 exhibited an oxidation onset ($E_{onset,ox}$) at 0.30 V and a reduction onset ($E_{onset,red}$) at −1.37 V, as shown in Figure 1a. The corresponding HOMO and LUMO levels were

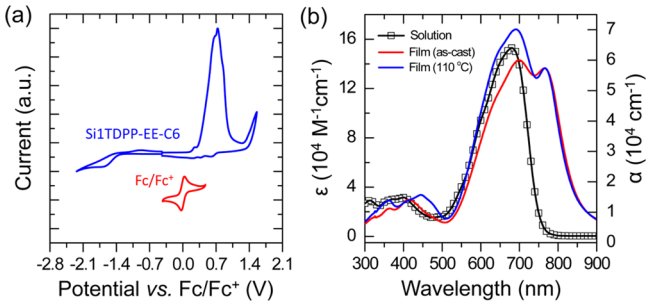

Figure 1. (a) A cyclic voltammogram obtained from a Si1TDPP-EE-C6 film along with a ferrocene/ferrocenium redox curve. (b) UV−visible absorption spectra of Si1TDPP-EE-C6 in solution and in the film state.

−5.10 and −3.43 eV, respectively. The electrochemical energy gap ($E_{g,cv}$) was 1.67 eV. These data suggest that a hole injection from Au electrodes (work function ~5.1 eV) to the Si1TDPP-EE-C6 channel would be preferable to an electron injection. Figure 1b presents UV−visible absorption spectra in solution and in the thin film state. A solution containing Si1TDPP-EE-C6 displayed a strong absorption band over the range 500−780 nm with a maximum absorption at 678 nm. An optical bandgap ($E_{g,opt}$) of 1.65 eV was obtained from the onset of the absorption spectrum in solution. The absorption of the film displayed a large red shift with an absorption onset of 840 nm (1.48 eV). This observation suggested that there are strong intermolecular interactions among the Si1TDPP-EE-C6 molecules with a molecular stacking of "phase I" (see below GIXD section for details). Upon thermal annealing at 110 °C, the absorption band over the range 500−750 nm became more intense, while the intensity of the absorption band at longer wavelengths did not change. This change suggested that the molecular stacking switched to more-ordered and well-packed "phase II" while film crystallinity was increased. The optical electronic properties are summarized in Table 1. Differential scanning calorimetry (DSC) measurements exhibited a melting temperature (T_m) at 189 °C and a clear crystallization temperature (T_c) of 158 °C, as shown in Figure S3 in the Supporting Information.

To gain a deeper understanding of the electronic structure, electronic transitions, and molecular geometries of Si1TDPP-EE-C6, we conducted quantum mechanical calculations using density function theory (DFT) and time-dependent DFT (TD-DFT) methods (Figure 2). A simplified Si1TDPP-EE-C6

Table 1. Redox Potentials, HOMO/LUMO Levels, and Bandgaps of Si1TDPP-EE-C6

	$E_{onset,ox}$ (V)	$E_{onset,red}$ (V)	HOMO[a] (eV)	LUMO[b] (eV)	$E_{g,cv}$[c] (eV)	$E_{g,opt}$[d] (eV)
Si1TDPP-EE-C6	0.30	−1.37	−5.10	−3.43	1.67	1.65

[a]HOMO = −($E_{onset,ox}$ + 4.8) eV. [b]LUMO =−($E_{onset,red}$ + 4.8) eV. [c]$E_{g,cv}$= (LUMO −HOMO) eV. [d]$E_{g,opt}$ was determined from the onset of the UV−visible absorption spectra in solution.

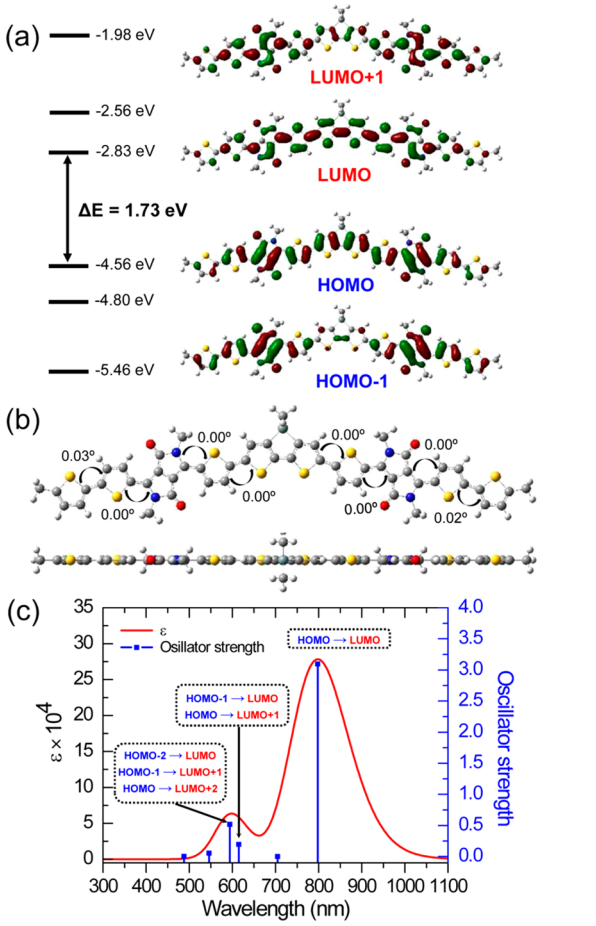

Figure 2. (a) Energy levels (left) and frontier molecular orbitals of the simplified Si1TDPP-EE-C6 (right). (b) Molecular geometry of the energy-minimized simplified Si1TDPP-EE-C6 molecule with dihedral angles. (c) UV−visible absorption spectrum of the simplified Si1TDPP-EE-C6 (red), which is based on the TD-DFT (B3LYP) calculations of the transition energy and oscillator strength (blue).

molecule, in which the alkyl chains were shortened to methyl groups, was geometrically optimized to an energy minimum using Gaussian 09 at the DFT B3LYP level with the 6-31+G(d,p) basis set. The HOMO and LUMO surface plots of the simplified Si1TDPP-EE-C6 molecule revealed highly delocalized orbitals along the molecular backbone (Figure 2a). The optimized molecular geometries indicated that the molecular backbone was quite flat (Figure 2b). The low dihedral angles ensured effective overlap among the π-orbitals, which reduced the optical bandgap and facilitated tight intermolecular packing (see below, the discussion of the GIXD data). The TD-DFT calculations predicted a UV−visible spectral shape (Figure 2c) that agreed well with the spectral shape obtained from Si1TDPP-EE-C6 in solution. Thus, the transitions from (HOMO−2 and HOMO−1) to LUMO and (HOMO−1 and HOMO) to LUMO+1 were found to be responsible for the absorption band observed at short wavelengths. The HOMO-to-LUMO transition with a high oscillator strength was found to be responsible for the absorption band observed at longer wavelengths.

dx.doi.org/10.1021/am500080p | ACS Appl. Mater. Interfaces 2014, 6, 6589−6597

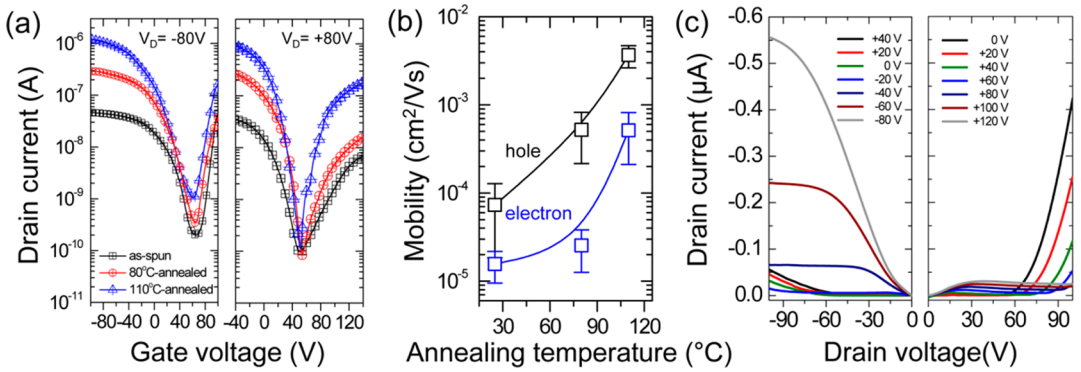

Figure 3. (a) Transfer characteristics at a fixed V_D of −80 V or +80 V for Si1TDPP-EE-C6 OFETs annealed at three temperatures: 25, 80, 110 °C. (b) Hole and electron mobilities of Si1TDPP-EE-C6 OFETs as a function of the annealing temperature. (c) Output characteristics of OFETs based on 110 °C-annealed Si1TDPP-EE-C6 films.

Bottom-gate top-contact organic field−effect transistors (OFETs) were prepared to evaluate the electrical properties of the Si1TDPP-EE-C6 layers. Figure 3a shows the transfer characteristics (drain current (I_D) − gate voltage (V_G)) at drain voltages (V_D) of −80 or +80 V, for Si1TDPP-EE-C6-based OFETs annealed at three temperatures: 25 (as-spun), 80, 110 °C. Ambipolar behavior were clearly displayed in the hole−enhancement at V_D = −80 V and electron−enhancement operational modes where V_D = −80 V and V_D = +80 V, respectively. The carrier mobilities were estimated in the respective saturation regimes according to the relationship $I_D = C_i\mu W(V_G - V_{th})^2/2L$, where W and L are the channel width and length, respectively, C_i is the specific capacitance of the gate dielectric (11 nF/cm^2), V_{th} is the threshold voltage, and μ is the carrier mobility. An OFET based on the as-spun Si1TDPP-EE-C6 exhibited average hole and electron mobilities of 7.3×10^{-5} and 1.6×10^{-5} cm^2/(Vs), respectively. Thermal annealing of the Si1TDPP-EE-C6 films considerably increased the carrier mobilities. The carrier mobilities of the device are summarized in Table 2 and their trend is shown in Figure 3b. The average

Table 2. Carrier Mobilities of OFETs Based on the Si1TDPP-EE-C6 at Three Annealing Temperatures

	25 °C	80 °C	110 °C
hole mobility (cm^2/(V s))	7.3 (± 5.5) × 10^{-5}	5.2 (± 3.0) × 10^{-4}	3.7 (± 1.0) × 10^{-3}
electron mobility (cm^2/(V s))	1.6 (± 0.6) × 10^{-5}	2.5 (± 1.3) × 10^{-5}	5.1 (± 3.0) × 10^{-4}

hole and electron mobilities of the OFETs based on the 110 °C-annealed Si1TDPP-EE-C6 film were 3.7×10^{-3} and 5.1×10^{-4} cm^2/(V s), respectively. Note that the hole mobility was high compared to the mobilities obtained from other DPP-based small molecules,[37,41−44] and this molecule is the second example of solution-processable small molecules that showed ambipolar behavior.[37] The enhanced carrier mobilities can be attributed to the increased intermolecular stacking of Si1TDPP-EE-C6 film (discussed below). Figure 3c shows the output characteristics (I_D−V_D) associated with hole or electron accumulation in the 110 °C-annealed Si1TDPP-EE-C6 OFETs. These curves displayed typical ambipolar characteristics: diode-like behavior at a low gate bias and saturation behavior at a high gate bias. The asymmetry between the hole and electron conduction properties was associated primarily with a greater efficiency in hole injection and a less efficiency in electron injection, from the Au to the Si1TDPP-EE-C6 molecular channel, because of the energy level alignment between the Fermi level of the Au electrode and the molecular HOMO/LUMO levels.

The microstructure of the Si1TDPP-EE-C6 thin film, which influenced the OFET performance, was characterized using synchrotron GIXD measurements. Figure 4a shows the GIXD images of the as-spun and 110 °C-annealed molecular films. The as-spun film exhibited a strong (100) diffraction peak with second and third order peaks and a weak (010) reflection along the out-of-plane (q_z) direction, whereas a (010) diffraction peak was clearly observed along the in-plane (q_y) direction. Thermal annealing of the molecular film at 110 °C resulted in more intense (h00) peaks along the q_z direction and (010) peaks along the q_y direction with the other diffraction peaks in the q_{yz} plane as well.

The GIXD patterns were analyzed in detail by extracting the 1D profiles along the q_z and q_y directions. Figure 4b shows the out-of-plane profiles extracted along the q_z direction at q_y = 0.00 Å^{-1} for the GIXD patterns of the Si1TDPP-EE-C6 films. The as-cast Si1TDPP-EE-C6 film showed strong (h00) diffraction peaks that corresponded to a $d_{(h00)}$ spacing of 15.6 Å, while the 110 °C-annealed Si1TDPP-EE-C6 film showed more pronounced (h00)′ reflections with higher order peaks that corresponded to a $d_{(h00)'}$ spacing of 18.9 Å. The $d_{(h00)'}$ spacing was nearly the same as the molecular width, i.e., the distance between the terminal carbon atom and the terminal carbon atom in the ethylhexyl groups on the DPP units. The in-plane profile, which was extracted along the q_y direction at q_z = 0.03 Å^{-1} (Figure 4c), revealed that upon annealing, the (h00) peaks disappeared and the (h00)′ peaks appeared. This result was consistent with the results obtained from the out-of-plane profile. Moreover, the (010) peak, which corresponded to a $d_{(010)}$ spacing of 3.7 Å, disappeared, whereas an intense (010)′ peak, which corresponded to a $d_{(010)'}$ spacing of 3.5 Å, appeared.

These GIXD results indicated that thermal annealing induced the Si1TDPP-EE-C6 films to undergo a phase transition from an ordered phase I, with $d_{(h00)}$ = 15.6 Å and $d_{(010)}$ = 3.7 Å, to a well-ordered and tightly stacked phase II, with $d_{(h00)}$ = 18.9 Å and $d_{(010)}$ = 3.5 Å. At the same time, thermal annealing promoted the development of an edge-on orientation among the crystalline Si1TDPP-EE-C6 molecules, in which π−π stacking interactions among the molecular backbones were oriented parallel to the substrate and the side alkyl chains pointed upward and downward. It was further corroborated by comparing the molecular width to the lamellar

dx.doi.org/10.1021/am500080p | ACS Appl. Mater. Interfaces 2014, 6, 6589−6597

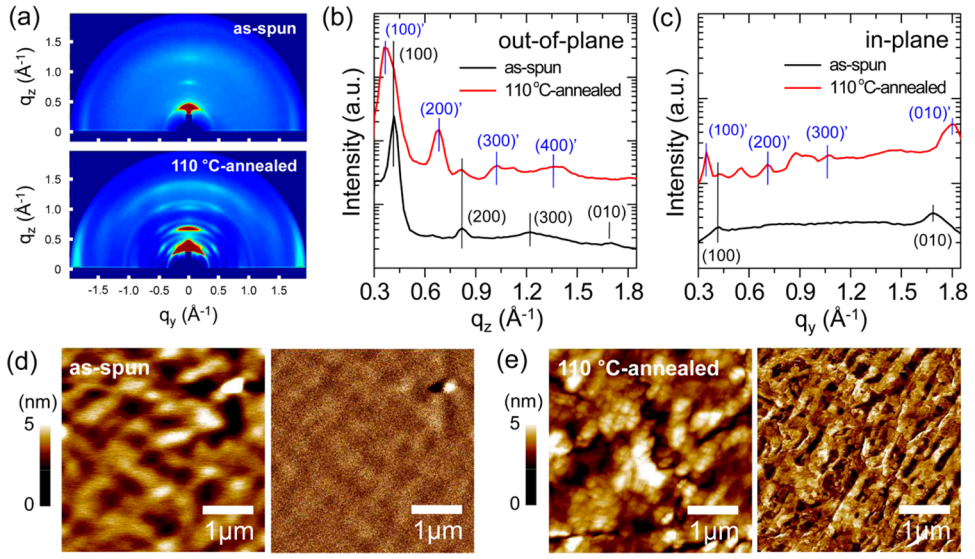

Figure 4. (a) GIXD patterns obtained from the as-spun (top) or 110 °C-annealed (bottom) Si1TDPP-EE-C6 films, (b) Out-of-plane X-ray diffraction profiles extracted along the q_z direction at q_y = 0.00 Å^{-1}, (c) In-plane X-ray diffraction profiles along the q_y direction at q_z = 0.03 Å^{-1}, (d) AFM topographic (left) and phase (right) images of the as-spun Si1TDPP-EE-C6 film, and (e) AFM topographic (left) and phase (right) images of the 110 °C-annealed Si1TDPP-EE-C6 film.

spacing measured in the phase II. It should be noted that the overall features of the well-stacked edge-on oriented Si1TDPP-EE-C6 molecules in the phase II provided an explanation for the improved hole mobility upon thermal annealing: well-ordered close $\pi-\pi$ stacking interactions would benefit charge transport along the semiconducting channel parallel to the substrate.

The surface morphologies of the as-spun or 110 °C-annealed Si1TDPP-EE-C6 films were examined. Images d and e in Figure 4 show the topographic and phase images of the corresponding films, respectively. The as-spun Si1TDPP-EE-C6 films exhibited featureless morphologies, whereas the films that were thermally annealed at 110 °C induced the crystalline nanostructures among the Si1TDPP-EE-C6 molecules. The enhanced crystalline nanostructures resulted in the increase of the surface roughness from 0.5 to 7.4 nm. Collectively, the GIXD and AFM images demonstrated that thermal annealing significantly impacted the molecular film morphology and offered an explanation for the observed Si1TDPP-EE-C6 OFET device performances.

Si1TDPP-EE-C6 layers were also used to fabricate nonvolatile memory devices. Figure 5a shows the device structure where AuNPs embedded at the interfaces between the *c*PVP and SiO_2 layer acted as charge trapping sites. The memory hysteresis loop was obtained from the nonvolatile memory based on 110 °C-annealed Si1TDPP-EE-C6, which demonstrates the dependence of V_G sweep range on the memory hysteresis property. At the V_G sweep from +20 to −20 V, the Si1TDPP-EE-C6 OFETs fabricated on the *c*PVP/AuNPs/SiO_2 exhibited unipolar p-type transistor behavior with a lower hole mobility (4.9×10^{-4} cm^2/(Vs)) compared to the Si1TDPP-EE-C6 OFETs prepared on the ODTS-treated SiO_2 gate dielectrics. The lower hole mobility and the absence of electron conduction were attributed to the relatively high number of electron trap sites of the *c*PVP/AuNPs/SiO_2. Figure 5c summarizes the change in memory window that was determined by the shifts in the threshold voltages (V_{th}) between the forward and reverse V_G sweeps, as a function of the V_G sweep range. During the V_G sweep from +20 to −20 V,

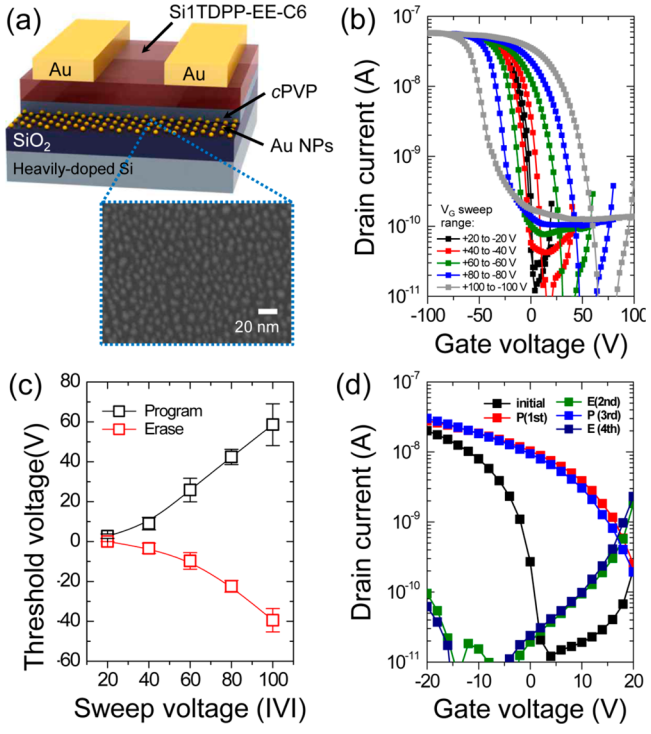

Figure 5. (a) Schematic diagram of the configuration of a Si1TDPP-EE-C6-based nonvolatile memory device prepared with the *c*PVP/AuNPs/SiO_2 substrate. The lower panel shows SEM images of the 1 nm-thick AuNPs layer. (b) A memory hysteresis loop obtained from the nonvolatile memory device based on a 110 °C-annealed Si1TDPP-EE-C6 film (V_D = −40 V). (c) Change in memory window as a function of the applied V_G. (d) Shifts in the transfer curves at V_D = −40 V upon application of V_G = +100 V (program) or −100 V (erase).

a little significant bias hysteresis (2.7 V) was observed; however, a $V_G \geq \pm$ 30 V resulted in a reversible bias hysteresis with a reproducible negative V_{th} shift, and the memory windows of the devices increased significantly with increasing V_G. The ±100 V

dx.doi.org/10.1021/am500080p | ACS Appl. Mater. Interfaces 2014, 6, 6589−6597

sweep yielded a huge V_{th} hysteresis of 98 V. The memory windows of the devices depended strongly on the applied electric field at the gate electrode because the number of charge carriers injected into and trapped within the AuNPs increased with the applied electric filed. The number of trapped charges can be calculated using the equation $\Delta n = C_i \cdot \Delta V_{th}/e$, where C_i and e are the specific capacitance of the gate dielectric (9.8 nF/cm^2) and the element charge, respectively. The total number of trapped charges obtained at $V_G = \pm 100$ V was calculated to be approximately 2.5×10^{12} cm^{-2}. The calculated number of trapped charges was strongly correlated with the AuNP density, which was estimated based on the SEM images, as shown in the lower panel of Figure 5a. The AuNP density was found to be roughly 1.2×10^{12} cm^{-2}. This number indicated that two electrons, on average, were stored in one AuNP. Figure 5d shows the reversible shifts in the transfer curves after the application of a program (P) voltage of $V_G = +100$ V and an erase (E) voltage of $V_G = -100$ at a $V_D = 0$ V for 1 s. That is, when the device was subjected to a programmed V_G of +100 V, the hole carriers injected from the AuNPs to the Si1TDPP-EE-C6 layer accumulated at the dielectric/organic interface to produce a high conductivity and a positive V_{th} shift. By contrast, the application of a negative V_G of −100 V for erasure resulted in the transfer of hole carriers at the Si1TDPP-EE-C6/cross-linked PVP interface to the AuNPs. The trapped hole charges in the AuNPs resulted in a low conductivity and a negative V_{th} shift.

The retention time and cycling tests were performed to characterize the operational stability of the Si1TDPP-EE-C6 nonvolatile memory device. Figure 6a presents the retention

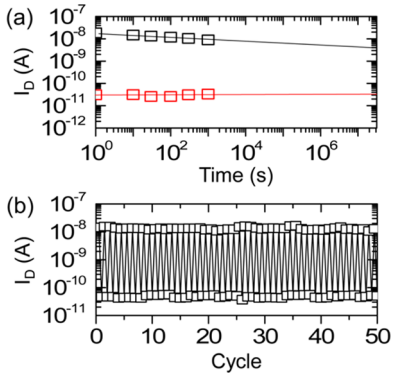

Figure 6. (a) Retention time and (b) cycling tests of nonvolatile memory devices based on Si1TDPP-EE-C6.

characteristics of the devices. The retention time was determined to exceed 10^8 s after application of a $V_G = \pm$ 100 V. The P/E states were maintained during repeated cycling tests, which included 50 cycles with a switching speed of 1 s (Figure 6b). These results demonstrated the good stability and reversibility of the Si1TDPP-EE-C6 nonvolatile memory device.

4. CONCLUSIONS

We demonstrate the synthesis and characterization of a low bandgap dithienosilole-cored semiconducting small molecule, Si1TDPP-EE-C6. The as-spun Si1TDPP-EE-C6 exhibited a low carrier mobility that improved significantly upon thermal annealing. The hole and electron mobilities of devices prepared from the 110 °C-annealed Si1TDPP-EE-C6 films were found to be 3.7×10^{-3} and 5.1×10^{-4} cm^2/(V s), respectively. The enhancement of the OFET performance was strongly correlated with the enhanced crystalline nanostructures in the semiconducting films via thermal treatment. Si1TDPP-EE-C6 was tested for its utility in nonvolatile memory devices. A Si1TDPP-EE-C6 memory device exhibited reliable nonvolatile memory characteristics, including a wide memory window of 98 V, a high on/off-current ratio of 1×10^3, and good electrical reliability. Note that this is the first report demonstrating that solution-processable small molecules can be applied in both ambipolar transistors and nonvolatile memory devices.

■ ASSOCIATED CONTENT

Ⓢ Supporting Information

^{1}H NMR spectrum, MALDI-TOF spectrum, and DSC thermogram of Si1TDPP-EE-C6. This material is available free of charge via the Internet at http://pubs.acs.org.

■ AUTHOR INFORMATION

Corresponding Authors

*E-mail: bongsoo@kist.re.kr. Tel: +82 2 958 5516. Fax: +82 2 958 6649.

*E-mail: jhcho94@skku.edu. Tel.: +82 31 299 4165. Fax: +82 31 299 4119,

Author Contributions

#W.K. and M.J. contributed equally to this work.

Notes

The authors declare no competing financial interest.

■ ACKNOWLEDGMENTS

This work was supported by New and Renewable Energy Program of the Korea Institute of Energy Technology Evaluation and Planning (KETEP) grant funded by the Korea Government Ministry of Trade, Industry & Energy (MTIE) (20113030010060), and by Korea Research Council of Fundamental Science and Technology (KRCF) and Korea Institute of Science and Technology (KIST) for "NAP National Agenda Project Program" (Project 2E23821), and by the National Research Foundation of Korea Grant funded by the Korean Government (MSIP) (2013, University-Institute corporation program), the Basic Research Program through the National Research Foundation of Korea (NRF) funded by the Ministry of Education, Science and Technology (2009-0083540), and the World-Class 300 Project (Development of organic materials with high transmittance, high insulating properties, and high flexibility for next generation display) funded by the Small and Medium Business Administration of Korea (SMBA).

■ REFERENCES

(1) Chua, L.-L.; Zaumseil, J.; Chang, J.-F.; Ou, E. C.-W.; Ho, P. K.-H.; Sirringhaus, H.; Friend, R. H. General Observation of N-Type Field-Effect Behaviour in Organic Semiconductors. *Nature* **2005**, *434*, 194−199.

(2) Yan, H.; Chen, Z.; Zheng, Y.; Newman, C.; Quinn, J. R.; Dötz, F.; Kastler, M.; Facchetti, A. A High-Mobility Electron-Transporting Polymer for Printed Transistors. *Nature* **2009**, *457*, 679−686.

(3) Zaumseil, J.; Sirringhaus, H. Electron and Ambipolar Transport in Organic Field-Effect Transistors. *Chem. Rev.* **2007**, *107*, 1296−1323.

(4) Zhang, W.; Smith, J.; Watkins, S. E.; Gysel, R.; McGehee, M.; Salleo, A.; Kirkpatrick, J.; Ashraf, S.; Anthopoulos, T.; Heeney, M. Indacenodithiophene Semiconducting Polymers for High-Perform-

ance, Air-Stable Transistors. *J. Am. Chem. Soc.* **2010**, *132*, 11437−11439.
(5) de Gans, B. J.; Duineveld, P. C.; Schubert, U. S. Inkjet Printing of Polymers: State of the Art and Future Developments. *Adv. Mater.* **2004**, *16*, 203−213.
(6) Sirringhaus, H.; Tessler, N.; Friend, R. H. Integrated Optoelectronic Devices Based on Conjugated Polymers. *Science* **1998**, *280*, 1741−1744.
(7) McCulloch, I.; Heeney, M.; Bailey, C.; Genevicius, K.; MacDonald, I.; Shkunov, M.; Sparrowe, D.; Tierney, S.; Wagner, R.; Zhang, W. Liquid-Crystalline Semiconducting Polymers with High Charge-Carrier Mobility. *Nat. Mater.* **2006**, *5*, 328−333.
(8) Dimitrakopoulos, C. D.; Malenfant, P. R. Organic Thin Film Transistors for Large Area Electronics. *Adv. Mater.* **2002**, *14*, 99−117.
(9) Beaujuge, P. M.; Pisula, W.; Tsao, H. N.; Ellinger, S.; Müllen, K.; Reynolds, J. R. Tailoring Structure-Property Relationships in Dithienosilole-Benzothiadiazole Donor-Acceptor Copolymers. *J. Am. Chem. Soc.* **2009**, *131*, 7514−7515.
(10) Cho, J. H.; Lee, J.; Xia, Y.; Kim, B.; He, Y.; Renn, M. J.; Lodge, T. P.; Frisbie, C. D. Printable Ion-Gel Gate Dielectrics for Low-Voltage Polymer Thin-Film Transistors on Plastic. *Nat. Mater.* **2008**, *7*, 900−906.
(11) Usta, H.; Facchetti, A.; Marks, T. J. N-Channel Semiconductor Materials Design for Organic Complementary Circuits. *Acc. Chem. Res.* **2011**, *44*, 501−510.
(12) Bronstein, H.; Chen, Z.; Ashraf, R. S.; Zhang, W.; Du, J.; Durrant, J. R.; Shakya Tuladhar, P.; Song, K.; Watkins, S. E.; Geerts, Y. Thieno[3, 2-b]thiophene− Diketopyrrolopyrrole-Containing Polymers for High-Performance Organic Field-Effect Transistors and Organic Photovoltaic Devices. *J. Am. Chem. Soc.* **2011**, *133*, 3272−3275.
(13) Crouch, D. J.; Skabara, P. J.; Lohr, J. E.; McDouall, J. J.; Heeney, M.; McCulloch, I.; Sparrowe, D.; Shkunov, M.; Coles, S. J.; Horton, P. N. Thiophene and Selenophene Copolymers Incorporating Fluorinated Phenylene Units in the Main Chain: Synthesis, Characterization, and Application in Organic Field-Effect Transistors. *Chem. Mater.* **2005**, *17*, 6567−6578.
(14) Lei, T.; Cao, Y.; Zhou, X.; Peng, Y.; Bian, J.; Pei, J. Systematic Investigation of Isoindigo-Based Polymeric Field-Effect Transistors: Design Strategy and Impact of Polymer Symmetry and Backbone Curvature. *Chem. Mater.* **2012**, *24*, 1762−1770.
(15) Mei, J.; Kim, D. H.; Ayzner, A. L.; Toney, M. F.; Bao, Z. Siloxane-Terminated Solubilizing Side Chains: Bringing Conjugated Polymer Backbones Closer and Boosting Hole Mobilities in Thin-Film Transistors. *J. Am. Chem. Soc.* **2011**, *133*, 20130−20133.
(16) Bijleveld, J. C.; Zoombelt, A. P.; Mathijssen, S. G.; Wienk, M. M.; Turbiez, M.; de Leeuw, D. M.; Janssen, R. A. Poly (Diketopyrrolopyrrole-Terthiophene) for Ambipolar Logic and Photovoltaics. *J. Am. Chem. Soc.* **2009**, *131*, 16616−16617.
(17) Lee, J. S.; Son, S. K.; Song, S.; Kim, H.; Lee, D. R.; Kim, K.; Ko, M. J.; Choi, D. H.; Kim, B.; Cho, J. H. Importance of Solubilizing Group and Backbone Planarity in Low Band Gap Polymers for High Performance Ambipolar Field-Effect Transistors. *Chem. Mater.* **2012**, *24*, 1316−1323.
(18) Tsao, H. N.; Cho, D. M.; Park, I.; Hansen, M. R.; Mavrinskiy, A.; Yoon, D. Y.; Graf, R.; Pisula, W.; Spiess, H. W.; Müllen, K. Ultrahigh Mobility in Polymer Field-Effect Transistors by Design. *J. Am. Chem. Soc.* **2011**, *133*, 2605−2612.
(19) Guo, X.; Kim, F. S.; Seger, M. J.; Jenekhe, S. A.; Watson, M. D. Naphthalene Diimide-Based Polymer Semiconductors: Synthesis, Structure-Property Correlations, and N-Channel and Ambipolar Field-Effect Transistors. *Chem. Mater.* **2012**, *24*, 1434−1442.
(20) Lee, H.-S.; Lee, J. S.; Cho, S.; Kim, H.; Kwak, K.-W.; Yoon, Y.; Son, S. K.; Kim, H.; Ko, M. J.; Lee, D.-K. Crystallinity-Controlled Naphthalene-Alt-Diketopyrrolopyrrole Copolymers for High-Performance Ambipolar Field Effect Transistors. *J. Phys. Chem. C* **2012**, *116*, 26204−26213.
(21) Lee, J.; Han, A.-R.; Kim, J.; Kim, Y.; Oh, J. H.; Yang, C. Solution-Processable Ambipolar Diketopyrrolopyrrole−Selenophene Polymer with Unprecedentedly High Hole and Electron Mobilities. *J. Am. Chem. Soc.* **2012**, *134*, 20713−20721.
(22) Sonar, P.; Singh, S. P.; Li, Y.; Soh, M. S.; Dodabalapur, A. A Low-Bandgap Diketopyrrolopyrrole-Benzothiadiazole-Based Copolymer for High-Mobility Ambipolar Organic Thin-Film Transistors. *Adv. Mater.* **2010**, *22*, 5409−5413.
(23) Zhou, E.; Yamakawa, S.; Tajima, K.; Yang, C.; Hashimoto, K. Synthesis and Photovoltaic Properties of Diketopyrrolopyrrole-Based Donor− Acceptor Copolymers. *Chem. Mater.* **2009**, *21*, 4055−4061.
(24) Sirringhaus, H.; Kawase, T.; Friend, R.; Shimoda, T.; Inbasekaran, M.; Wu, W.; Woo, E. High-Resolution Inkjet Printing of All-Polymer Transistor Circuits. *Science* **2000**, *290*, 2123−2126.
(25) Braga, D.; Erickson, N. C.; Renn, M. J.; Holmes, R. J.; Frisbie, C. D. High-Transconductance Organic Thin-Film Electrochemical Transistors for Driving Low-Voltage Red-Green-Blue Active Matrix Organic Light-Emitting Devices. *Adv. Funct. Mater.* **2012**, *22*, 1623−1631.
(26) Facchetti, A. Π-Conjugated Polymers for Organic Electronics and Photovoltaic Cell Applications. *Chem. Mater.* **2010**, *23*, 733−758.
(27) Crone, B.; Dodabalapur, A.; Lin, Y.-Y.; Filas, R.; Bao, Z.; LaDuca, A.; Sarpeshkar, R.; Katz, H.; Li, W. Large-Scale Complementary Integrated Circuits Based on Organic Transistors. *Nature* **2000**, *403*, 521−523.
(28) Meijer, E.; De Leeuw, D.; Setayesh, S.; Van Veenendaal, E.; Huisman, B.-H.; Blom, P.; Hummelen, J.; Scherf, U.; Klapwijk, T. Solution-Processed Ambipolar Organic Field-Effect Transistors and Inverters. *Nat. Mater.* **2003**, *2*, 678−682.
(29) Smith, J.; Bashir, A.; Adamopoulos, G.; Anthony, J. E.; Bradley, D. D.; Heeney, M.; McCulloch, I.; Anthopoulos, T. D. Air-Stable Solution-Processed Hybrid Transistors with Hole and Electron Mobilities Exceeding 2 $cm^2 V^{-1} s^{-1}$. *Adv. Mater.* **2010**, *22*, 3598−3602.
(30) Kim, F. S.; Guo, X.; Watson, M. D.; Jenekhe, S. A. High-Mobility Ambipolar Transistors and High-Gain Inverters from a Donor−Acceptor Copolymer Semiconductor. *Adv. Mater.* **2010**, *22*, 478−482.
(31) Dodabalapur, A.; Katz, H.; Torsi, L.; Haddon, R. Organic Heterostructure Field-Effect Transistors. *Science* **1995**, *269*, 1560−1562.
(32) Beaujuge, P. M.; Fréchet, J. M. Molecular Design and Ordering Effects in Π-Functional Materials for Transistor and Solar Cell Applications. *J. Am. Chem. Soc.* **2011**, *133*, 20009−20029.
(33) Li, Y. Molecular Design of Photovoltaic Materials for Polymer Solar Cells: Toward Suitable Electronic Energy Levels and Broad Absorption. *Acc. Chem. Res.* **2012**, *45*, 723−733.
(34) Coughlin, J. E.; Henson, Z. B.; Welch, G. C.; Bazan, G. C. Design and Synthesis of Molecular Donors for Solution-Processed High-Efficiency Organic Solar Cells. *Acc. Chem. Res.* **2013**, *47*, 257−270.
(35) Mei, J.; Diao, Y.; Appleton, A. L.; Fang, L.; Bao, Z. Integrated Materials Design of Organic Semiconductors for Field-Effect Transistors. *J. Am. Chem. Soc.* **2013**, *135*, 6724−6746.
(36) Arias, A. C.; MacKenzie, J. D.; McCulloch, I.; Rivnay, J.; Salleo, A. Materials and Applications for Large Area Electronics: Solution-Based Approaches. *Chem. Rev.* **2010**, *110*, 3−24.
(37) Zhang, Y.; Kim, C.; Lin, J.; Nguyen, T.-Q. Solution-Processed Ambipolar Field-Effect Transistor Based on Diketopyrrolopyrrole Functionalized with Benzothiadiazole. *Adv. Funct. Mater.* **2012**, *22*, 97−105.
(38) Chen, H.-Y.; Hou, J.; Hayden, A. E.; Yang, H.; Houk, K. N.; Yang, Y. Silicon Atom Substitution Enhances Interchain Packing in a Thiophene-Based Polymer System. *Adv. Mater.* **2010**, *22*, 371−375.
(39) Welch, G. C.; Bakus, R. C.; Teat, S. J.; Bazan, G. C. Impact of Regiochemistry and Isoelectronic Bridgehead Substitution on the Molecular Shape and Bulk Organization of Narrow Bandgap Chromophores. *J. Am. Chem. Soc.* **2013**, *135*, 2298−2305.
(40) Grisorio, R.; Allegretta, G.; Suranna, G. P.; Mastrorilli, P.; Loiudice, A.; Rizzo, A.; Mazzeo, M.; Gigli, G. Monodispersed Vs. Polydispersed Systems for Bulk Heterojunction Solar Cells: The Case

of Dithienopyrrole/Anthracene Based Materials. *J. Mater. Chem.* **2012**, *22*, 19752−19760.
(41) Loser, S.; Bruns, C. J.; Miyauchi, H.; Ortiz, R. P.; Facchetti, A.; Stupp, S. I.; Marks, T. J. A Naphthodithiophene-Diketopyrrolopyrrole Donor Molecule for Efficient Solution-Processed Solar Cells. *J. Am. Chem. Soc.* **2011**, *133*, 8142−8145.
(42) Walker, B.; Liu, J.; Kim, C.; Welch, G. C.; Park, J. K.; Lin, J.; Zalar, P.; Proctor, C. M.; Seo, J. H.; Bazan, G. C.; Nguyen, T.-Q. Optimization of Energy Levels by Molecular Design: Evaluation of Bis-Diketopyrrolopyrrole Molecular Donor Materials for Bulk Heterojunction Solar Cells. *Energy Environ. Sci.* **2013**, *6*, 952−962.
(43) Sonar, P.; Williams, E. L.; Singh, S. P.; Manzhos, S.; Dodabalapur, A. A Benzothiadiazole End Capped Donor-Acceptor Based Small Molecule for Organic Electronics. *Phys. Chem. Chem. Phys.* **2013**, *15*, 17064−17069.
(44) Tantiwiwat, M.; Tamayo, A.; Luu, N.; Dang, X.-D.; Nguyen, T.-Q. Oligothiophene Derivatives Functionalized with a Diketopyrrolopyrrolo Core for Solution-Processed Field Effect Transistors: Effect of Alkyl Substituents and Thermal Annealing. *J. Phys. Chem. C* **2008**, *112*, 17402−17407.